The Monte Carlo Method: Versatility Unbounded In A Dynamic Computing World
Chattanooga, Tennessee, April 17–21, 2005, on CD-ROM, American Nuclear Society, LaGrange Park, IL (2005)

THE UF FAMILY OF PEDIATRIC TOMOGRAPHIC MODELS

Choonik Lee and Wesley Bolch
Department of Nuclear Engineering
University of Florida
Gainesville, Florida 32611
choonik@ufl.edu; wbolch@ufl.edu

Jon Williams
Department of Radiology
University of Florida
Gainesville, Florida 32611
willjl@ufl.edu

ABSTRACT

The use of computed tomography (CT) in pediatric radiology has rapidly increased over the past 15 years. While CT accounts for only about 10% of diagnostic radiological exams, it contributes disproportionately to the patient collective dose. The issue of radiation risk is of far greater importance in pediatric radiology as children are inherently more radiosensitive than adults. Strategies for dose reduction, as well as optimization of image quality versus patient dose, are thus crucial in pediatric CT. While many indicator quantities are easily measured in the clinic (such as the CTDI or DLP), the effective dose is the most fundamental indicator of patient risk in pediatric CT, a quantity requiring knowledge of individual organ doses. The effective dose thus requires the use of heterogeneous anthropomorphic models of pediatric anatomy. While many tomographic models of adult anatomy have been developed over the past 15 years, relatively few models are of children as needed in medical CT dosimetry. Using both cadaver and live patient image sets, we have been developing a series of tomographic pediatric models for use in pediatric radiology. The current UF family of pediatric models currently stands at six models: 6-day female, 9-month male, 4-year female, 8-year female, 11-year male, and 14-year male. The newborn model was constructed from a cadaver scan, while the remaining models were developed from segmentation of head and chest-abdomen-pelvis (CAP) scans of live patients. In addition to their use in Monte Carlo simulations of CT, fluoroscopy, and projection radiography, physical phantoms of the UF newborn and UF 9-mo models have been constructed using tissue equivalent materials for soft tissue, lung, and bone. Internal placement of high-sensitivity MOSFET dosimeters at organ centroids, and Monte Carlo-derived point-to-organ dose scaling factors provide a means of physical verification of doses estimates via computer simulation.

Key Words: Tomographic models, pediatric radiology, organ dose, voxel model

1. INTRODUCTION

Of the many measures of patient radiation exposure in CT dosimetry, four quantities have been more frequently adopted and/or reported in the literature: the volumetric CT dose index ($CTDI_{vol}$), the dose-length product (DLP), the energy imparted (ε), and the effective dose (E) [1]. The $CTDI_{vol}$ represents the weighted average of both a central ($CTDI_C$ or $CTDI_{100}$) and peripheral ($CTDI_P$) measurement of air ionization within an acrylic cylindrical phantom ($CTDI_w$) normalized by the beam pitch ($CTDI_{vol} = CTDI_w / P$). The DLP is simply the product of the

$CTDI_{vol}$ and the effective axial length of the scan. Finally, the energy imparted is the total amount of photon energy deposited within a cylindrical phantom across the scan length (estimated as the product of the $CTDI_{vol}$ and the mass of irradiated phantom volume – or by computer simulation in a cylindrical water phantom). Consequently, all three quantities utilize very approximate physical representations of the patient anatomy (homogeneous cylinders), and each provides no direct information on radiation dose, and thus risk, to individual radiosensitive organs of the body (e.g., thyroid, bone marrow).

In contrast, the effective dose provides a far more direct measure of patient risk. The quantity E was introduced by the ICRP in 1990 [2], and represents a weighted average of the absorbed dose to individual organs of body ($E = \Sigma\ w_T\ \Sigma\ w_R\ D_{R,T}$). These organs include the breasts, lungs, reproductive organs (ovaries and testes), thyroid, active bone marrow, skeletal endosteum, esophageal wall, stomach wall, colon wall, liver, skin, and urinary bladder, and remainder tissues. The tissue weighting factors, w_T, needed to calculate E represent the fraction of total risk of radiation injury contributed by that particular tissue during radiation exposure, while weighting factors w_R represent the relative biological effectiveness of the radiation involved in that exposure. Values of organ and effective dose can only be obtained by direct physical measurement or computer simulation using phantoms or mathematical models of patients where individual internal organs are delineated [3]. Alternatively, these measurements or simulations may yield conversion coefficients (effective or organ dose per unit $CTDI_{vol}$ or per unit ε) which when multiplied by the indicator quantities ($CTDI_{vol}$ or ε) will provide estimates of individual patient values of E or organ dose. In fact, such an estimate of E is required as part of the annual physics surveys for the American College of Radiology CT Accreditation Program [4]. Unfortunately, the availability of these conversion coefficients is extremely limited, and those that do exist are (1) based upon very simplistic anatomic patient models, (2) are available primarily for only adult patients (thus requiring simplistic mass scaling for pediatric patients), and (3) are based upon single-detector scanning technology. Furthermore, computational models of pediatric patients with sufficient anatomic realism are extremely limited, and essentially no physical phantoms of this nature exist for which conversion coefficients and/or direct measurements of pediatric organ and effective dose can be made in real-time within clinical practice.

In the present study, we summary work performed in the UF Pediatric Organ Dose (POD) Project in which a full-body model of a newborn baby, as well as series of other pediatric tomographic models covering a range of ages and both genders, has been developed.

1.1 Construction of the UF Newborn Tomographic Computational Model

The software routine *CT_Contours* was developed in the UF Pediatric Organ Dose (POD) Project to facilitate image segmentation of CT data sets for construction of anatomic models of pediatric anatomy. The code, written using Interactive Data Language (IDL) version 5.5 (Research Systems, Inc., Boulder, CO) has been described previously in Nipper et al. (Appendix B) [5]. IDL was chosen over a more basic programming language such as C++ due to its inherit ability to handle image formats, its ease of use, and the ability to output data in a variety of formats. *CT_Contours* was designed to output labeled contour files as binary files for EGSnrc [6], as ASCII text for MCNP [7], and as bitmap files for creating templates for physical phantom construction [8].

CT_Contours was created so that future users can interactively create and manipulate contour data sets. The program takes advantage of many of the built-in functions of IDL and was created with an easy-to-use graphical user interface to minimize the need for future programming modifications (see Figs. 1 and 2). The program displays the current CT information, as well as a color overlay of the contours being edited. The contours can be displayed using a variety of different color schemes and transparencies, and they can be created using a variety of tools including basic thresholding, pixel growing, voxel growing, region growing, and manual segmentation. These segmentation methods can also be used in conjunction with one another, so that any segmentation errors that arise from the automatic routines can be corrected through manual drawing. The voxels contained in the individual contours are filled with the desired segmentation value, generating volumes of voxels with identical tag values representing individual organs or body regions.

The data available to construct our first newborn tomographic model consisted of 485 CT slices of a six-day-old female cadaver. The patient died in an attempt to correct congenital abnormalities of the great vessels, and was imaged within 24 hours of death. The CT data had been obtained from a whole-body helical scan, using a GE LightSpeed CT scanner. The image slices were contiguous, with no gaps or overlapping data. Each slice was saved as a 512 x 512 image, with an in-plane pixel resolution of 0.586 mm x 0.586 mm and a thickness of 1 mm. The cadaver mass had been recorded at 3.83 kg (8.4 lbs). The patient was imaged in the traditional supine position, with the scanner acquiring images in the transverse plane. Unlike most CT scans of live pediatric patients, the arms were positioned parallel to the body. The patient image set was examined and the patient was found to be free of any physical defects that would prevent its further use. The only abnormality was a moderate edema on the left parietal region of the head, which can be considered as representative of normal individual variability for newborn patients. The final model is shown graphically in Fig. 3.

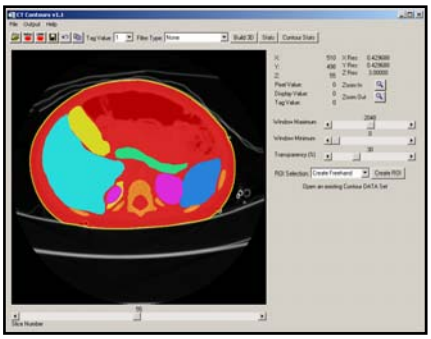

Figure 1.
Imaging processing code CT_Contours used to segment pixels within a 2D CT image into individual organs and tissue regions.

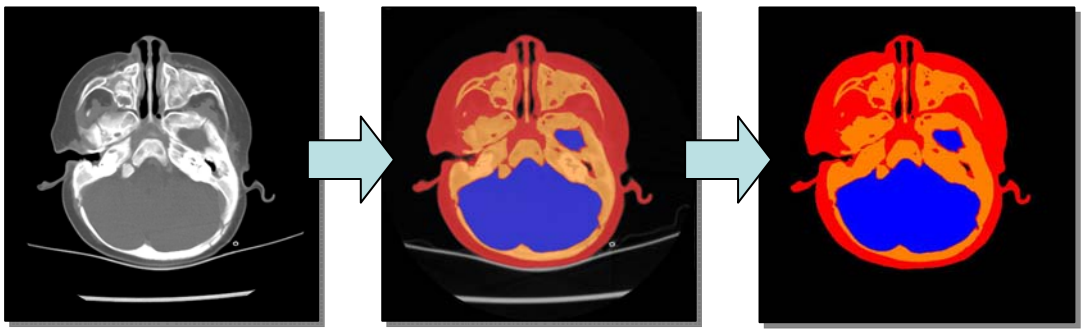

Figure 2. Representative steps in creating a slice within the tomographic model of the 9-mo male.

Figure 3. Anterior views of the UF newborn tomographic model.

The EGSnrc radiation transport code was selected for coupling to the newborn tomographic model due to its versatility in handling large voxelized arrays [6]. With a rectilinear array of 512 × 512 × 485 voxels, the newborn tomographic model is represented by a matrix of over 127 million individual voxels. Each voxel has a tag belonging to one of the 66 segmented regions. For each segmented region, the energy deposition was tracked across all voxels to report absorbed dose. For skeletal regions, the volume-averaged particle fluence (ratio of cumulative photon track length to skeletal site volume) was calculated with dose to both active marrow and endosteum obtained via fluence-to-dose conversions factors published by Eckerman [9]. Simulations are typically run with ~10 to 50 million initial particles. Photons are followed down to an energy of 1 keV and secondary electrons with kinetic energy below 10 keV deposited their energy locally.

1.2 Organ Doses in Newborn Radiography

In 2003, we reported in Staton et al. [10] estimates of individual organ doses received in four different newborn radiographic exams using both the stylized and newly available tomographic computational model. These exams were of the head, chest, abdomen, and thorax (chest/abdomen) representative of those performed in the Neonatal ICU of Shands Children's Hospital using GE AMX4 Mobile CR radiographic units. Radiographic techniques were selected based on standard pediatric technique charts posted in the NICU: 0.5 mAs, 102 mm SID, and kVp as a function of total patient mass (66 kVp in the case of the newborn models). Head radiographs are not typically performed in the NICU, but were included in the study for completeness. The TASMIP algorithm of Boone and Siebert [11] was used to generate the x-ray spectrum (2.33 mm Al HVL). As in clinical practice, the field sizes were determined by patient anatomy with the chest exam running from top of the trunk to the base of the lungs, and the abdomen exam running from the top of the kidneys to the base of the bladder and field widths were well collimated to the patient. A comparison of organ doses (weighted by w_T) within the AP and RLAT thorax radiographs are demonstrated for both models in Figs 4 and 5, respectively. Values of effective dose per unit entrance air-kerma are shown in Fig. 6.

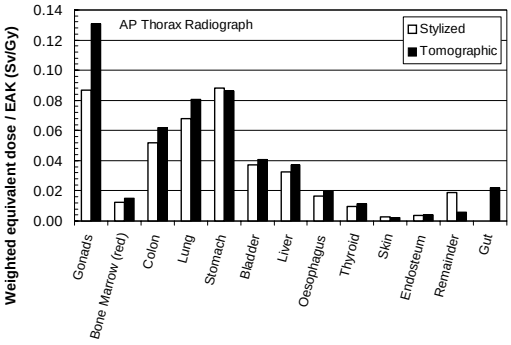

Figure 4. Organ dose per entrance air kerma free in air (Sv Gy^{-1}) for the AP thorax radiograph.

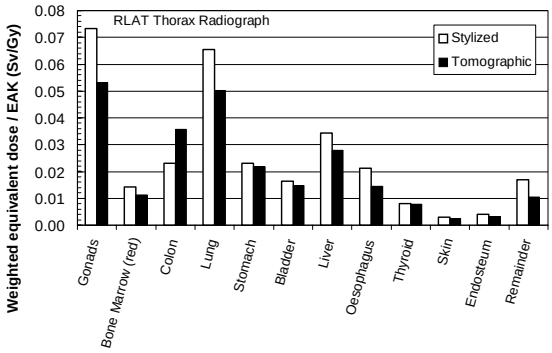

Figure 5. Organ dose per entrance air kerma free in air (Sv Gy^{-1}) for the RLAT thorax radiograph.

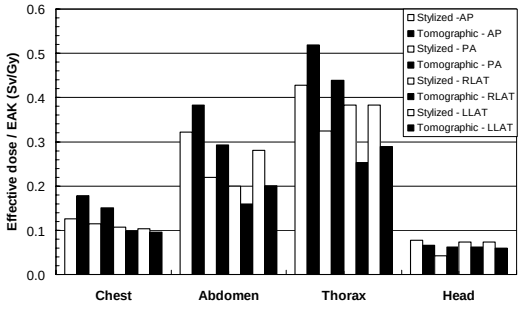

Figure 6. Effective dose per unit entrance air kerma free in air (Sv Gy^{-1}) for all sixteen radiographic exams.

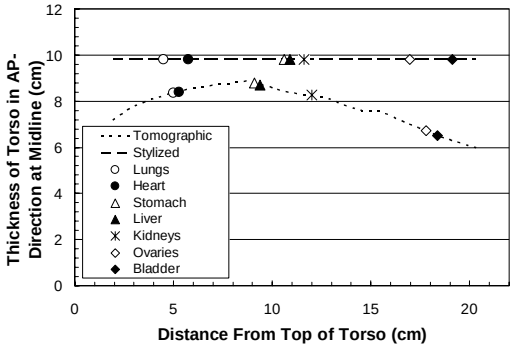

Fig 7. Thickness of torso in the AP-direction at the midline as a function of distance from the top of the torso. Points indicate the locations of the organ centroids.

For AP and PA radiographs of the torso (chest, abdomen, and thorax views), the effective dose assessed for the tomographic model exceeds that for the stylized model with percent differences ranging from 19% (AP abdominal view) to 43% AP chest view. In contrast, the effective dose for the stylized model exceeds that for the tomographic model for all eight lateral views including those of the head, with percent differences ranging from 9% (LLAT chest view) to 51% (RLAT thorax view). Overall, a major factor for differences in both effective and individual organ doses between the two models for similar projections/views is the unrealistic exterior trunk shape of the stylized model (see Figs 7 and 8). Even though differences do exist in individual organ positioning, their effects are overshadowed by those of overall exterior trunk shape. Figure 7 compares vertical organ positioning and midline trunk thickness in the AP direction in both the tomographic and stylized newborn models. The midline trunk thickness in the AP direction of the stylized model remains constant at ~9 cm, while this distance varies significantly over the length of the torso in the tomographic model with the greatest difference occurring in the abdominal region. Even though organs are positioned similarly in the vertical direction (abscissa of data points), the additional tissue thickness in the stylized model creates increased shielding for these organs for AP and PA thorax radiographs (ordinate of data points). In contrast, the thickness in the lateral direction of the tomographic model exceeds that of the stylized model throughout the length of the torso even with the arms removed. The exterior trunk shape of the tomographic model is more elliptical when compared to the stylized model, an observation that is opposite of that seen in tomographic and stylized models of the adult [12].

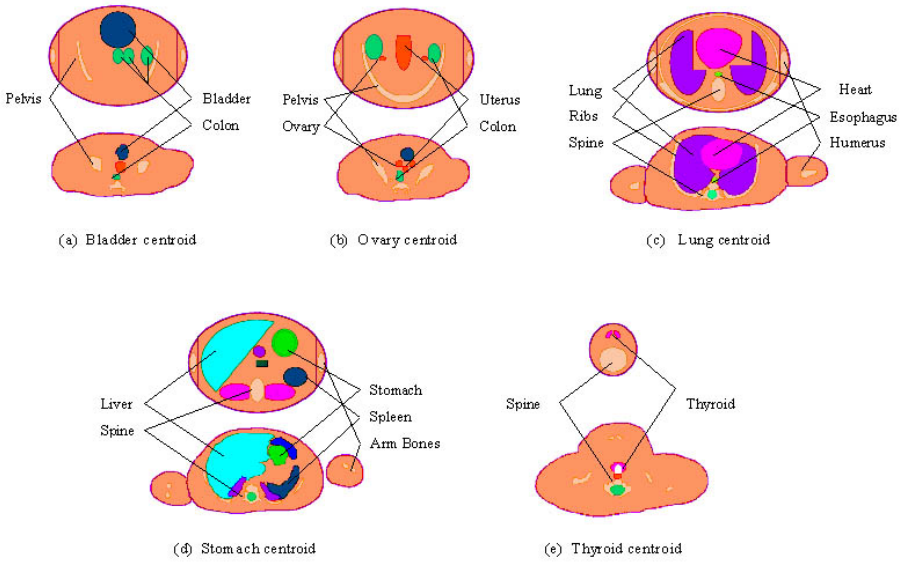

Figure 8.
Axial slices at the position of organ centroids within the newborn stylized (top) and tomographic (bottom) models: (a) bladder, (b) ovaries, (c) lungs, (d) stomach, and (e) thyroid. For each panel and model, the anterior surface is at the top, the posterior surface is at the bottom, and the left and right sides of the models are reversed as if viewed from the feet (standard CT image viewing).

1.3 Organ Doses in Newborn Multi-Slice CT

Recently, we have modified our radiographic simulation code for the *UF Newborn* model to simulate patient irradiation during multi-slice helical CT examination. The modified code allows for simulations of CT exams with a number of input parameters such as tube potential, pitch, collimated beam thickness, and scan coverage. The code has been written to simulate exposures using a Siemens SOMATOM Sensation 16 multi-slice helical CT scanner which is used for all CT scanning of pediatric patients within the Shands Children's Hospital. The x-ray spectra, explicit helical source motion, beam geometry, beam-shaping filtration, and beam profile have been modeled as accurately as possible to estimate individual organ doses for this particular CT scanner. Proprietary information, such as the technical specifications of the beam-shaping filter, have been provided to us directly from the manufacturer. The EGSnrc code calculates the absorbed dose (mGy) per launched x-ray photon for each of the 122 regions that have been segmented within the model. The x-ray fluence (number/cm^2) per launched photon is also calculated for each of the 33 segmented regions of the skeleton.

For organs other than bone tissues, an average organ dose is calculated using the energy deposited in the voxels of a given organ and the organ mass. For bone marrow and bone surface dose, a dose response function was used as tabulated by Eckerman for the ORNL series of stylized models [9, 13]. The dose response functions yield an active marrow dose or bone surface dose per unit x-ray fluence within each bone region. The dose response function is broken down into energy bins and skeletal regions (such as parietal and lumbar vertebra). Several improvements in skeletal dose response functions can be made, and these techniques will be explored further within the proposed research study.

The results of the Monte Carlo simulations provide organ dose per launched photon for each region in the tomographic model. To calculate absolute organ doses, the central CT dose index ($CTDI_C$ or $CTDT_{100}$) was measured and as well as simulated for each CT exam. As noted earlier, $CTDI_{100}$ is an indicator measurement of patient dose in CT using a cylindrical acrylic phantom. Radiation exposure is measured for a single CT slice at the center of the phantom using a 100-

mm pencil ionization chamber. $CTDI_{100}$ represents the absorbed dose in a small volume within the central slice of a multi-slice exam and accounts for scatter radiation from other slices.

In this study, $CTDI_{100}$ was evaluated using a 16-cm-diameter acrylic phantom which is used in clinical measurements to simulate a pediatric torso. A CT data set of the acrylic phantom was acquired and utilized in voxelized form for $CTDI_{100}$ simulations. The active volume of the ion chamber was modeled as air and the dose to air in the chamber was calculated via radiation transport simulation and yielding values of $CTDI_{100}$ per simulated x-ray photon. When combined with the newborn organ dose data for the same scan parameters, values of organ dose per unit $CTDI_{100}$ are generated. $CTDI_{100}$ measurements are also made for each set of scan parameters. Absolute organ doses are then calculated as the product of the organ dose per unit $CTDI_{100}$ (EGSnrc simulation) and the physical measurement of $CTDI_{100}$.

A total of sixteen CT simulations were recently completed and covered head, chest, abdomen, and pelvis scans with the following technique factors: 80 and 120 kVp, 12-mm collimated beam thickness, and pitch values of 1 and 1.5. All absolute organ doses and effective doses are normalized to a tube current of 100 mA and tube rotation time of 1 sec. All reported effective doses and organ doses within the scan field have an associated error of less than 1%. Figure 9 shows the results of effective dose for all sixteen CT scan simulations. The highest effective dose occurred for the chest scans with a maximum of 11.3 mSv at 120 kVp and a pitch value of 1. The lowest effective dose occurred in the head scans with a minimum of 1.03 mSv at 80 kVp and a pitch value of 1.5. For all scan types, the effective dose was found to vary inversely proportionate to the pitch as expected. The ratio of the effective doses at 80 and 120 kVp for a given scan was found to be approximately equal to the ratio of $CTDI_{100}$ values at 80 and 120 kVp. The $CTDI_{100}$ values for 80 and 120 kVp were measured be 6.3 mGy and 18.8 mGy, respectively. Figure 10 shows some of the highest individual organ doses per 100 mAs for CT chest scans at 80 and 120 kVp and a pitch value of 1. The lung and bone surface doses had the highest values with doses of 34.3 and 34.2 mGy respectively. Figure 11 shows organ dose data for CT head scans. The bone surface and bone marrow doses had the highest values with doses of 46.1 and 22.2 mGy respectively. Individual organ doses are shown to be reduced by a factor of up to 3 by reducing the tube potential from 120 to 80 kVp.

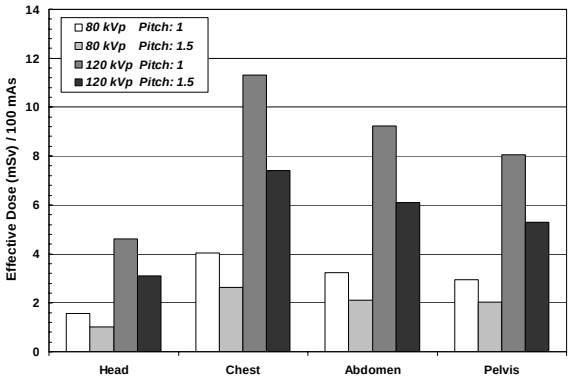

Figure 9. Total effective dose (mSv) per 100 mAs for all 16 CT exam simulations using the UF Newborn model.

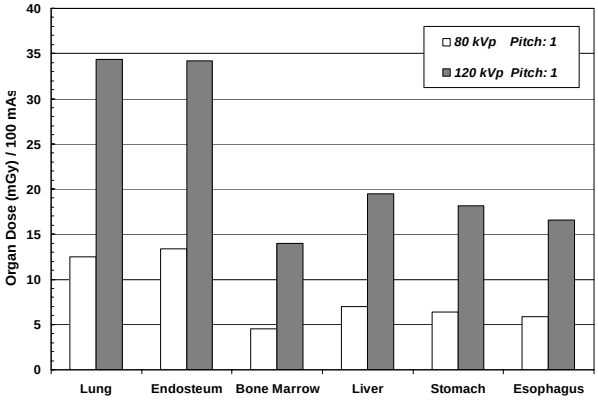

Figure 10. Organ doses (mGy) per 100 mAs for chest CT exam simulations at 80 and 120 kVp.

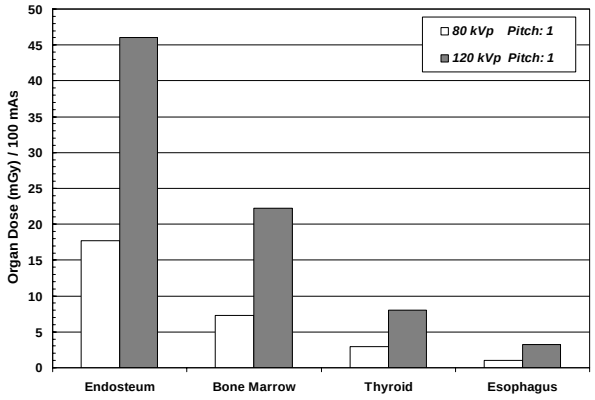

Figure 11. Organ doses (mGy) per 100 mAs for head CT exam simulations at 80 and 120 kVp.

1.4 Establishment of the UF Pediatric Model Series

Following the development of the CT_Contours segmentation software, and the construction of our first tomographic dosimetry model (UF Newborn), work has progressed over the past two years in expanding the family of pediatric models available for organ dose assessment in pediatric CT and other imaging modalities (our original grant proposed work only on a newborn model). Table 1 below summaries the current status of the UF family of tomographic models. Unlike the newborn model, these older models were constructed from image segmentation of archived medical images of live patients undergoing Head and CAP (Chest-Abdomen-Pelvis) CT examinations. As such, neither model includes the arms or legs within the medical scan; consequently, they are suitable for use in reconstruction studies of organ doses, where the arms and legs are out-of-field and receive only a small contribution of scattered radiation. While they do not posses the level of axial resolution obtained in the 6-day newborn model (cadaver based), the presence of CT contrast agent significantly enhanced our ability to see and thus segment various organs and organ regions. Examples include partitioning of the kidneys (renal cortex from renal medulla) and "remainder tissues" into muscle and adipose tissue. This latter achievement is significant in that these tissues (1) provide differential x-ray attenuation at diagnostic energies, (2) cannot be distinguished within stylized models, and (3) provide a basis for extending normal weight models to those of obese or underweight individuals – a feature totally devoid within the current series of stylized reference models. The entire model series beyond the UF Newborn is shown in Figure 12 below. A cross-sectional comparison of the ORNL 10-year stylized model and that of the UF 11-year male tomographic model is given in Figure 13.

Table 1. Current status of the UF pediatric family of tomographic dosimetry models.

Model Name	Gender	Image Source	Voxel Resolution	Current Status
UF Newborn	Female	Cadaver	0.59 x 0.59 x 1 mm	Complete
UF 9-mo	Male	CT Scan - Head and CAP	0.43 x 0.43 x 3 mm	Complete
UF 4-yr	Female	CT Scan – Head and CAP	0.45 x 0.45 x 5 mm	Complete
UF 8-yr	Female	CT Scan – Head and CAP	0.58 x 0.58 x 6 mm	Complete
UF 11-yr	Male	CT Scan – Head and CAP	0.47 x 0.47 x 6 mm	Complete
UF 14-yr	Male	CT Scan – Head and CAP	0.62 x 0.62 x 6 mm	Complete

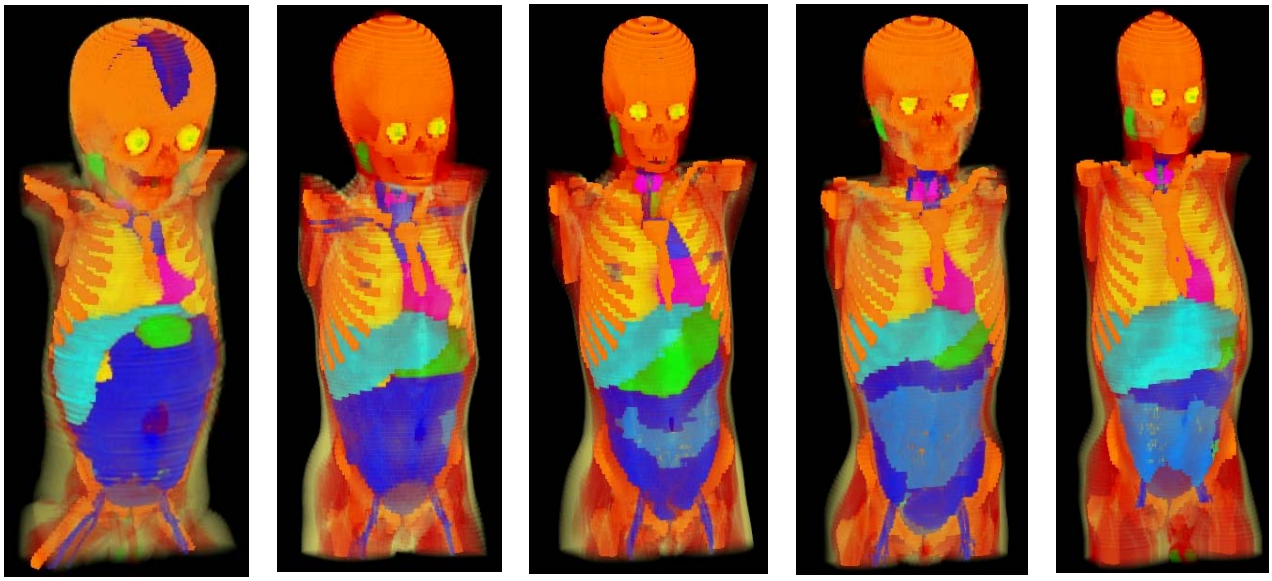

Figure 12. UF pediatric tomographic model series. From left to right are the 9-mo male, 4-year female, 8-year female, 11-year male, and 14-year male anatomic models.

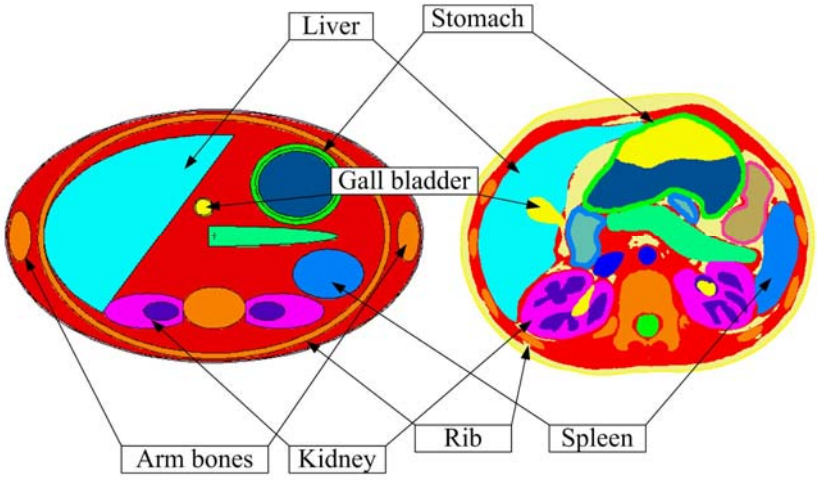

Figure 13. Transverse images from the stylized model ORNL 10-year model and the UF 11-year male model.

2 CONCLUSIONS

Five head-torso tomographic computational models of different ages (9-month male, 4-year female, 8-year female, 11-year male, and 14-year male) have been constructed from the CT images of live patients for subsequent use in radiation dosimetry studies in pediatric radiology. The models were created from fused images taken from head CT and CAP CT exams of the same individuals (9-month and 4-year models) or two different individuals of the same sex with close age (8-year, 11-year, and 14-year models). A physical tomographic phantom of the UF Newborn and UF 9-month male model have recently been constructed using the tissue equivalent materials developed in our research group. Monte Carlo simulations and physical measurements using these models/phantoms will permit improved patient dose reconstructions.

3 ACKNOWLEDGMENTS

This work was support by grant RO1 EB00267 from the National Institute for Biomedical Imaging and Bioengineering (NIBIB) with the University of Florida.

4 REFERENCES

1. M. Prokop. Radiation dose and image quality. In: Prokop, M.; Galanski, M., eds. *Spiral and multislice computed tomography of the body*. New York: Thieme Publishers; 2003:131-160.
2. ICRP. *1990 Recommendations.* Publication 60. International Commission on Radiological Protection; 1991.
3. C. Suess, X. Chen. Dose optimization in pediatric CT: current technology and future innovations. *Pediatr Radiol* (2002) 32:729-34; discussion 751-4.
4. American College of Radiology. *CT Accreditation Program Requirements.* www.acr.org.
5. J. Nipper, J. Williams, W. Bolch. Creation of two tomographic voxel models of pediatric patients in the first year of life. *Phys Med Biol* (2002) 47:3143-3164.
6. I. Kawrakow. Accurate condensed history Monte Carlo simulation of electron transport. I. EGSnrc, the new EGS4 version. *Med Phys* (2000) 27:485-498.
7. J. F. Briesmeister. *MCNP - A general Monte Carlo N-particle transport code.* LA-12625-M. Los Alamos National Laboratory; 1997.
8. J. Sessions, J. Roshau, M. Tressler, D. Hintenlang, M. Arreola, J. Williams, W. Bolch. Comparisons of point and average organ dose within an anthropomorphic physical phantom and a computational model of the newborn patient. *Med Phys* (2002) 29:1080-1089.
9. K. F. Eckerman. Aspects of the dosimetry of radionuclides within the skeleton with particular emphasis on the active marrow. In: Schlafke-Stelson, A.T.; Watson, E.E., eds. *Proceedings of the Fourth International Radiopharmaceutical Dosimetry Symposium*. Oak Ridge, Tennessee: Oak Ridge Associated Universities; CONF-85113, 1985:514-534.
10. R. Staton, F. Pazik, J. Nipper, J. Williams, and W. Bolch. A comparison of newborn stylized and tomographic models for dose assessment in pediatric radiology. *Phys Med Biol* (2003) 48:805-820.
11. J. M. Boone, J. A. Seibert. An accurate method for computer-generating tungsten anode x-ray spectra from 30 to 140 kV. *Med Phys* (1997) 24:1661-1670.
12. M. Zankl, U. Fill, N. Petoussi-Henss, D. Regulla. Organ dose conversion coefficients for external photon irradiation of male and female voxel models. *Phys Med Biol* (2002) 47:2367-85.
13. M. Cristy, K. F. Eckerman. *Specific absorbed fractions of energy at various ages from internal photon sources.* ORNL/TM-8381/Volumes I-VII. Oak Ridge National Laboratory; 1987.
14. A.K. Jones, D. E. Hintenlang, W. E. Bolch. Tissue-equivalent materials for construction of tomographic dosimetry phantoms in pediatric radiology. *Medical Physics* (2003) 30:2072-2081.